Towards Fully Autonomous Driving: Systems and Algorithms

Jesse Levinson, Jake Askeland, Jan Becker, Jennifer Dolson, David Held, Soeren Kammel,
J. Zico Kolter, Dirk Langer, Oliver Pink, Vaughan Pratt, Michael Sokolsky,
Ganymed Stanek, David Stavens, Alex Teichman, Moritz Werling, and Sebastian Thrun

***Abstract*— In order to achieve autonomous operation of a vehicle in urban situations with unpredictable traffic, several realtime systems must interoperate, including environment perception, localization, planning, and control. In addition, a robust vehicle platform with appropriate sensors, computational hardware, networking, and software infrastructure is essential.**

We previously published an overview of Junior, Stanford's entry in the 2007 DARPA Urban Challenge.[1] This race was a closed-course competition which, while historic and inciting much progress in the field, was not fully representative of the situations that exist in the real world. In this paper, we present a summary of our recent research towards the goal of enabling safe and robust autonomous operation in more realistic situations.

First, a trio of unsupervised algorithms automatically calibrates our 64-beam rotating LIDAR with accuracy superior to tedious hand measurements. We then generate high-resolution maps of the environment which are subsequently used for online localization with centimeter accuracy. Improved perception and recognition algorithms now enable Junior to track and classify obstacles as cyclists, pedestrians, and vehicles; traffic lights are detected as well. A new planning system uses this incoming data to generate thousands of candidate trajectories per second, choosing the optimal path dynamically. The improved controller continuously selects throttle, brake, and steering actuations that maximize comfort and minimize trajectory error.

All of these algorithms work in sun or rain and during the day or night. With these systems operating together, Junior has successfully logged hundreds of miles of autonomous operation in a variety of real-life conditions.

I. INTRODUCTION

Fully autonomous driving in real urban settings has remained an important but elusive goal. Many notable attempts have been made, and several important milestones have been reached. Perhaps the most famous was the 2007 DARPA Urban Challenge, in which teams from across the world designed the hardware and software for autonomous vehicles that could handle dynamic obstacles, intersections, and merging. In the event, over 50 robotic and non-robotic vehicles drove simultaneously on a closed course for an entire day, and six robots successfully completed the race. Our lab's entry, an autonomous Volkswagen Passat named "Junior," was among the winners.

While the Urban Challenge remains the largest demonstration of autonomous vehicle technology to date, it excluded many capabilities and requirements critical for actual driving in cities. Specifically, it was closed to pedestrians and bicyclists, featured wide roads with speeds under 35 MPH, had no traffic lights, and enforced only a subset of the many rules detailed by the Department of Motor Vehicles. Finally, DARPA officials were allowed to pause, interrupt, and restart individual vehicles in the race in order to minimize risk and enable smoother operation.

Fig. 1. Junior: Stanford's autonomous research vehicle.

In parallel, over the last several decades, many attempts have been made to operate an autonomous vehicle on public streets. In general, these efforts have been restricted to a subset of the full driving task; e.g. highway-only, parking-only, or throttle/brake only. [2]

In this paper, we describe a variety of algorithmic improvements and solutions that our lab has implemented on Junior since the Urban Challenge, all of which are motivated by the goal of safer, more competent driving in a variety of real on-road situations. Many of the individual results have been published recently, and as we are presenting a wide variety of ideas here, this paper can be considered a brief overview of our entire system as it has evolved over the last three years.

II. SYSTEM AND VEHICLE

A. Hardware

Our research vehicle is a 2006 Volkswagen Passat wagon (Figure 1). This remains an ideal platform, providing plenty of space for equipment and people, as well as featuring an electronically actuated throttle, shifter, parking brake, and steering system. An interface box designed in collaboration with VW provides software control over these functions as well as brake pressure and turn signals, in addition to the ability to fall back to human control of the vehicle during a software or power failure, or by manual takeover.

The current suite of sensors includes a Velodyne HDL-64E S2 rotating 64-beam LIDAR and four cameras from Point Grey: a Ladybug3 spherical camera, two color Flea2's for forward stereo vision, and a Grasshopper for high resolution forward monocular vision. Also present are 6 Bosch automotive radars covering the front, rear, and side views, two SICK LD-LRS LIDAR scanners covering the blind spots, and an Applanix POS-LV 420 inertial GPS navigation system.

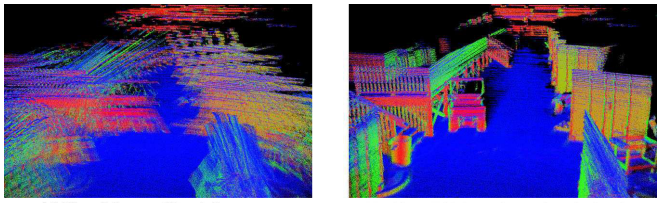

(a) Horribly uncalibrated sensor. (b) After 300 iterations of optimization

Fig. 2. Unsupervised intrinsic calibration using 10 seconds of data (all scans depicted above). Points colored by surface normal. Even starting with an unrealistically inaccurate calibration (a) we are still able to achieve a very accurate calibration after optimization (b).

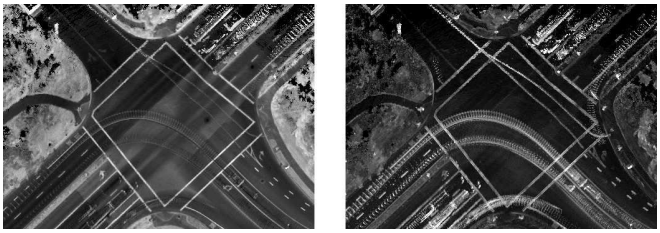

Fig. 3. The two channels of our probabilistic maps. On the left we see the average infrared reflectivity, or brightness, of each cell. Our approach is novel in also considering the extent to which the brightness of each cell varies, as shown on the right.

Two on-board Xeon computers running Linux provide more than enough processing power; a 12-core server runs our vision and laser algorithms while a 6-core server takes care of planning, control, and low-level communication.

B. Software

The low-level software system is a modified version of that used in the 2005 DARPA Grand Challenge and the 2007 Urban Challenge. Individual input, output, and processing modules run asynchronously, communicating over network sockets and shared memory. This paper focuses on modules developed since the Urban Challenge; for a more in-depth treatment of the initial system, see [1].

Significant changes have been made, primarily to enable a shift in focus from competition-mode to research. Unlike in a competition, in which software is expected to recover or restart no matter what, in a research vehicle deployed in real-world environments, safety is the primary concern. Thus, a safety driver is always present behind the wheel, taking over whenever there is a software issue or unexpected event.

In the sections that follow, we will discuss the various algorithms and modules that have changed significantly since our previous report.

III. Unsupervised Laser Calibration

Whereas single-beam sensors can often be calibrated without great difficulty, deriving an accurate calibration for lasers with many simultaneous beams has been a tedious and significantly harder challenge. We have developed a fully unsupervised approach to multi-beam laser calibration [3], recovering optimal parameters for each beam's orientation and distance response function. Our method allows simultaneous calibration of tens or hundreds of beams, each with its own parameters. In addition, we recover the sensor's extrinsic pose relative to the robot's coordinate frame.

Crucially, our approach requires no specific calibration target, instead relying only on the weak assumption that points in space tend to lie on contiguous surfaces. Specifically, we define an energy function on point clouds which penalizes points that are far away from surfaces defined by points from other beams:

$$J = \sum_{b_i=1}^{B} \sum_{b_j=b_i-N}^{b_i+N} \sum_{k} w_k \|\eta_k \cdot (p_k - m_k)\|^2$$

where B is the total number of beams and N is the number of neighboring beams we align each beam to, k iterates over the points seen by beam b_j, p_k is the kth point projected according to the current transform, m_k is the closest point to p_k seen by beam b_i, η_k is the surface normal at point m_k and w_k is 1 or 0 based on whether $\|p_k - m_k\| < d_{max}$

For the intrinsic calibration, we aggregate points acquired across a series of poses, and take derivatives of the energy function across pairs of beams with respect to individual parameters. Using an iterative optimization method we arrive a globally consistent calibration that is more accurate than the factory calibration, even with an unrealistically bad initialization (see Figure 2).

For the extrinsic calibration of the LIDAR's mounting location on the vehicle, the same energy function is used, but in this case an iterative application of grid search is used to discover the optimal 6-DOF sensor pose. Here, we can recover the position within 1 cm, and the orientation to within a much finer granularity than can be measured by hand.

Finally, we also calibrate the intensity remittance return values for each beam by using Expectation Maximization to enforce the constraint that beams should roughly agree on the (unknown) brightness of surfaces in the environment. The resulting remittance maps are significantly more consistent after calibration.

IV. Mapping and Localization

Autonomous vehicle navigation in dynamic urban environments requires localization accuracy exceeding that available from GPS-based inertial guidance systems. Although the Urban Challenge prohibited pre-driving the course, no such limitation exists in the real world; thus, we use GPS, IMU, and Velodyne LIDAR data to generate a high-resolution infrared remittance ground map that can be subsequently used for localization. [4] For algorithmic and computational simplicity, our maps are orthographic grid-based projections of LIDAR remittance returns onto the ground plane.

Our approach yields substantial improvements over previous work in vehicle localization, including higher precision, the ability to learn and improve maps over time, and increased robustness to environment changes and dynamic obstacles. Specifically, we model the environment, instead of as a spatial grid of fixed infrared remittance values, as a probabilistic grid whereby every cell is represented as its own gaussian distribution over remittance values; see Figure 3. Subsequently, Bayesian inference is able to preferentially weight parts of the map most likely to be stationary and of

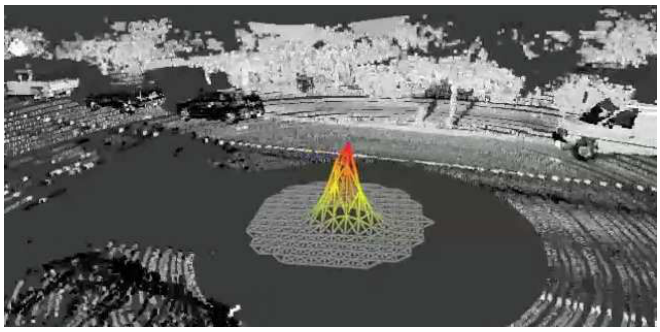

Fig. 4. A realtime 2-dimensional histogram showing the posterior belief about our vehicle's location; the current Velodyne scan is also shown.

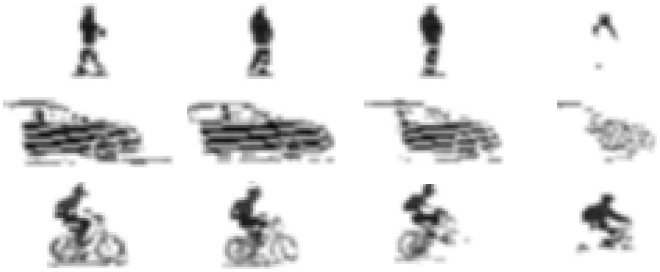

Fig. 5. Virtual orthographic camera intensity images from three tracks of objects that Junior can recognize. Depth segmentation of objects provides invariance to background clutter. Classification of depth data allows one to put objects in a canonical orientation, thus providing some measure of perspective invariance.

consistent angular reflectivity, thereby reducing uncertainty and catastrophic errors. Furthermore, by using offline SLAM to align multiple passes of the same environment[5], possibly separated in time by days or even months, it is possible to build an increasingly robust understanding of the world that can be then exploited for localization.

Given a pre-recorded laser map and live incoming LIDAR data, we alternatively employ Bayesian motion and measurement updates to a 2D histogram filter which tracks the offset of the vehicle's intertial coordinate frame to the global UTM coordinates of the map; see Figure IV.

Localizing our vehicle against these probabilistic maps in various dynamic environments, we achieve lateral RMS accuracy better than 10cm, which is sufficiently precise for any public road. In hundreds of miles of testing, we have experienced no catostrophic localization failures with this system.

V. Object recognition

In some scenarios, an autonomous vehicle requires deeper understanding of the environment to behave correctly; for example, at intersections, knowing the location of pedestrians and bicyclists can allow the car to make more sophisticated precedence decisions.

Junior's object recognition system now includes recognition of pedestrians, bicyclists, and cars. The following is a brief overview of the key points of this system; see [6] for details.

First, every Velodyne scan is segmented using depth information. This essentially amounts to local ground plane removal and connected components clustering of the remaining points, done in a 2D grid for efficiency. The segments are then fed into a standard Kalman tracker which includes (x, y) position and $(\dot{x}, \dot{y})$ velocity in its state variable. Classification of *tracks* of objects was found to be essential to high performance.

Track classification is done by applying two separate boosting classifiers: one of the shape of the object at each frame in the track, and one on motion descriptors of the entire track. These predictions are combined using a discrete Bayes filter. Example frame descriptors are shown in Figure 5.

When tracking and segmentation are correct, the accuracy of the classifier is about 98% overall. The system is able to run in real time due to caching of shared computation in the descriptor pipeline and because classification of only segmented objects dramatically reduces the number of possibilities that must be considered compared to sliding window type approaches. By only considering objects near the road and those that were previously recognized as pedestrians, bicyclists, and cars, we are frequently able to classify everything in every scan while maintaining real time operation.

Failures of the segmentation and tracking components are currently the primary limitations of the objects recognition system. For example, when a pedestrian presses a crosswalk button, he is segmented in with the pole it is mounted on and he is not recognized. We hope to explore more advanced segmentation and tracking methods in the future.

VI. Trajectory Planning

As autonomous vehicles advance toward handling realistic road traffic, they face street scenarios where the dynamics of other traffic participants must be considered explicitly. These situations include everyday driving maneuvers like merging into traffic flow, passing with on- coming traffic, changing lanes, or avoiding other vehicles. This is where trajectory concepts come into play, which explicitly account for the time on the planning and execution level. The presented method embarks on this strategy and transfers velocity and distance control to the planning level. Additionally, the algorithm provides for reactive obstacle avoidance by the combined usage of steering and breaking/acceleration [7].

We formulate the problem of trajectory tracking in an optimal sense to take advantage of optimal control theory asserting consistency in the choice of the best feasible trajectory over time. For the car, this means that it follows the remainder of the previously calculated trajectory in each planning step. Bellman's Principle therefore asserts convergence.

While our main criterion in choosing a cost functional is compliance with Bellman's principle of optimality, trajectories minimizing it must still be close to the desired traffic behavior of the autonomous car. At the same time, the best compromise has to be found in the longitudinal direction in an analog manner. Assuming the car drives too fast or too close to the vehicle in front, it has to slow down noticeably but without excessive rush. Ease and comfort can be best described by the derivative of lateral or longitudinal acceleration: $\text{jerk}(t) := \dot{a}(t)$.

A well known approach in tracking control theory is the moving frame method [8]. Here, we use the Frenet-Serret formulation and apply the moving frame method for combining different lateral and longitudinal cost functionals for different tasks as well as to mimic human-like driving behavior. The moving reference frame is given by the tangential and normal vectors at a certain point of some curve referred to as the *center line* in the following. This center line represents either the ideal path along the free road, or the result of a path planning algorithm for unstructured environments [9]. Rather than formulating the trajectory generation problem directly in Cartesian Coordinates, we switch to the above mentioned dynamic reference frame and seek to generate a one-dimensional trajectory for both the root point along the center line and the perpendicular offset.

1) Lateral Motion: Since we seek to maximize comfort and therefore minimize the squared jerk along the resulting trajectory, we choose the start state of our optimization according to the previously calculated trajectory. The cost functional

$$C_d = k_j \int_{t_0}^{t_1} \dddot{d}(\tau)\mathrm{d}\tau + k_t[t_1 - t_0] + k_d d_1^2 \qquad (1)$$

with d_1 as the lateral deviation at the end state of the current planning horizon, and the weighting factors $k_j, k_t, k_d > 0$, is independent of the longitudinal movement and therefore velocity invariant. Quintic polynomials can be found to satisfy this cost functional. Instead of calculating the best trajectory explicitly and modifying the coefficients to get a valid alternative, we generate in a first step, such as in [10], a trajectory set by combining different end conditions. In a second step we can pick the valid trajectory with the lowest cost. Notice that, as we continue in each step along the optimal trajectory, the remaining trajectory will be, the optimal solution in the next step. At extreme low speeds, this strategy above disregards the non-holonomic property of the car, so that the majority of the trajectories would be rejected due to invalid curvatures. For this reason the behavioral layer can switch below a certain velocity threshold to a slightly different trajectory mode generating the lateral trajectory in dependence on the longitudinal movement; see [7] for details.

2) Longitudinal Movement: In contrast to previous works where time or travelled distance was the key criterion, we will focus here on comfort and contribute at the same time to safety at high speeds, as smooth movements adapt much better to the traffic flow. For that reason, we also take the longitudinal jerk into account in our optimization problem. Since distance keeping, merging, and stopping at certain positions require trajectories, which describe the transfer from the current position to a longitudinal, possibly moving, target position, we generate a longitudinal trajectory set analogously to the lateral trajectories with the following cost functional:

$$C_t = k_j \int_{t_0}^{t_1} \dddot{s}(\tau)\mathrm{d}\tau + k_t[t_1 - t_0] + k_s[s_1 - s_d]^2\,, \qquad (2)$$

with the distance to the leading vehicle along the center line s_d. Again, a quintic polynomials satisfies the cost functional. The movement of the leading vehicle has to be predicted within the considered time horizon. Similarly, we can define a target point which enables us to position the autonomous car next to a pair of vehicles before squeezing slowly in between during a tight merging maneuver. For stopping at intersections due to a red light or a stop sign, the target distance becomes the distance to the stop line and the target's velocity and acceleration are set to 0.

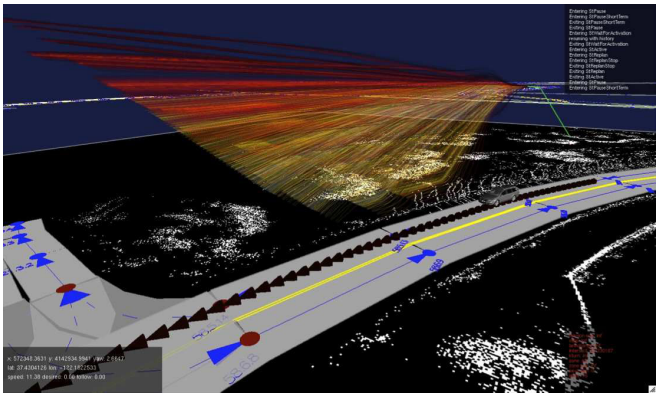

Fig. 6. Smooth trajectory set: The z axis shows the velocity; overall costs are indicated by the color.

In situations without a vehicle or a stop line directly ahead, the autonomous car does not necessarily have to be at a certain position but needs to adapt to a desired velocity given by the behavioral level. For this case, the cost functional

$$C_v = k_j \int_{t_0}^{t_1} \dddot{s}(\tau)\mathrm{d}\tau + k_t[t_1 - t_0] + k_{\dot{s}}[\dot{s}_1 - \dot{s}_d]^2\,, \qquad (3)$$

is satisfied by a quartic polynomial. Before combining the lateral and longitudinal trajectory sets, each one is checked against outsized curvatures and acceleration values. The remainders in each set are then brought together in every combination.

3) Combining Lateral and Longitudinal Curves: In a last step, the conjoint costs of each trajectory is calculated as the weighted sum:

$$C_{\text{tot}} = k_{\text{lat}} C_{\text{lat}} + k_{\text{lon}} C_{\text{lon}} \qquad (4)$$

As far as our experience goes, it is sufficient for highway trajectory generation to classify all traffic scenarios as merging, following another car, keeping a certain velocity, stopping at a certain point, and all combinations thereof, which are conflicting most of the time. In control theory, override control is a well-known technique, which chooses among multiple control strategies according to a scheme, prevalently the most conservative one via a max or a min operator. An example for a generated smooth trajectory set is shown in Fig. 6.

VII. Dynamical Modeling and Control

The goal of Junior's control system is to take the upcoming trajectory output by the planner and generate system inputs (throttle/braking and steering torque) in order to follow this trajectory. To achieve this end, we employ a mixture of a model predictive control (MPC) strategy, based upon well-known physically based vehicle models [11], along with

feedforward proportional integral derivative (PID) control for the lower-level feedback control tasks such as applying torque to achieve a desired wheel angle.

At the higher of these two levels, the car's state and control input are described by the vectors $\mathbf{x} \in \mathbb{R}^7$ and $\mathbf{u} \in \mathbb{R}^2$

$$\mathbf{x} = [x, y, \theta, u, v, \dot{\theta}, \delta], \quad \mathbf{u} = [\dot{u}, \dot{\delta}] \tag{5}$$

where x, y, and θ denote the 2D state and orientation, u and v denote the longitudinal and lateral velocities (aligned with the car frame), δ denotes the wheel angle, and the dotted variables represent the corresponding time derivatives. The equations of motion are given by a bicycle model[1]

$$\begin{aligned} \dot{v} &= \tan\delta(\dot{u} - \dot{\theta}v) + (F_{yf}/\cos\delta + F_{yr})/m - \dot{\theta}u \\ I\ddot{\theta} &= ma\tan\delta(\dot{u} - \dot{\theta}v) + aF_{yf}/\cos\delta - bF_{yr} \end{aligned} \tag{6}$$

where m denotes the car's mass a and b denote the distance from the center of gravity to the front and rear axles respectively, I is the moment of inertia, and the lateral tire forces are given via a linear tire model with stiffness C,

$$F_{yf} = C\left(\tan^{-1}\left(\frac{v + \dot{\theta}a}{u}\right) - \delta\right), F_{yf} = C\tan^{-1}\left(\frac{v - \dot{\theta}b}{u}\right). \tag{7}$$

Given this system, we interpret a trajectory output by the planner as a sequence of desired states $\mathbf{x}^\star_{1:H}$ for some time horizon H, and minimize the quadratic cost function

$$J(\mathbf{u}_{1:H}) = \sum_{t=1}^{H} \left((\mathbf{x}_t - \mathbf{x}^\star_t)^T Q(\mathbf{x}_t - \mathbf{x}^\star_t) + \mathbf{u}_t^T R\mathbf{u}_t\right) \tag{8}$$

subject to the system dynamics, where Q and R are cost matrices (chosen to be diagonal, in our case), that specify the trade-off in errors between the different state components. We minimize this objective by linearizing the dynamics around the target trajectory, and applying an algorithm known as the Linear Quadratic Regulator (LQR) [13] to the resulting linearized system; this optimization is done in an online fashion, each time we send a new control command.

Finally, after obtaining controls that approximately minimize this cost function, we integrate the dynamics forward, leading to a sequence of desired steering angles and velocities $\delta^d_{1:H}, u^d_{1:H}$ (and similarly for their velocities). To achieve these states we use feedforward PID control, for instance applying steering torque

$$\tau = k_p(\delta_t - \delta^d_t) + k_d(\dot{\delta} - \dot{\delta}^d) + k_{ff} f(\delta^d_t) \tag{9}$$

where k_p, k_d and k_{ff} are the feedback gains, and $f(\delta)$ is a feedforward control tuned for the car.

VIII. Traffic Light Detection

Detection of traffic light state is essential for autonomous driving in urban environments. We have developed a passive camera-based pipeline for traffic light state detection, using vehicle localization and assuming prior knowledge of traffic light location [14]. In order to achieve robust real-time detection results in a variety of lighting conditions, we combine several probabilistic stages that explicitly account for the corresponding sources of sensor and data uncertainty. In addition, our approach is the first to account for multiple lights per intersection, which yields superior results by probabilistically combining evidence from all available lights. These techniques have for the first time enabled our autonomous research vehicle to successfully navigate through traffic-light-controlled intersections in real traffic.

[1]Although not usually written in this form, this is simply the model from e.g. [12] for a front wheel drive car and with the longitudinal forces set to whatever value necessary to achieve $\dot{u}$ acceleration.

Fig. 7. Simultaneous detection of three distinct traffic lights at one intersection. The left turn lights do not affect our lane, so are not considered.

To overcome the limitations of purely vision-based approaches, we take advantage of temporal information, tracking and updating our estimate of each light's image coordinates and state using a histogram filter. To somewhat constrain our traffic light search region, we pre-map traffic light locations and therefore assume that a prior on the global location of traffic lights is available during detection, utilizing pose data available from a GPS system.

Tight search regions also provide us the precision required to detect the state of multiple traffic lights within an intersection (see Figure 7) and treat each light as an independent measurement of the true intersection state. When combined, we can expect improved robustness to several pathological situations, like superfluous lights and temporary occlusions.

A condensed version of our pipeline for state detection of a single traffic light is as follows:

1) Supply the module with a pre-defined list of global traffic light locations.
2) Begin looking for lights at a distance determined by the camera resolution and vehicle braking distance.
3) Project a region of interest, centered on the expected location of the traffic light, onto the camera frame.
4) Apply a template-matching algorithm to the region of interest.
5) Multiply the result into a histogram filter and blur to account for uncertainty.
6) Report the light's image coordinates as that of the maximum valued cell in the filter.
7) Report the light's state as red, yellow, or green, depending on the hue of the cell at the light's image coordinates.

IX. Generic Sign Detection and Direction-Invariant Stop Sign Classification

State-of-the-art autonomous vehicles today continue to depend on manually constructed road maps to provide the location of all traffic signs. To automate this process, we have built a laser-based generic sign detector, which locates

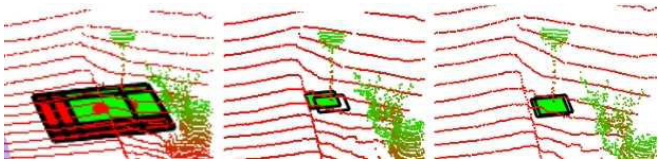

Fig. 8. Left: Multiple detections for a single sign, before non-maximal suppression. Center: a single detection for a single sign, after non-maximal suppression. Right: A single sign detection, re-centered using the weighted average of the classification values.

the position and orientation of all signs surrounding the autonomous vehicle. We have also implemented a direction-invariant classifier that can distinguish stop signs from non-stop signs, even when viewed from the back or side, which can help an autonomous car differentiate from a 2-way stop vs a 4-way stop.

Given a 3d point cloud, an SVM is trained to detect all signs of all types around the car. Negative examples are obtained using feedback retraining in a similar manner to that in [15]. To compute the features for the SVM, the points within each square are divided into 0.5 m sections based on height, referenced by the lowest point in each square. Features are computed both overall for the square, as well as separately for each height section. Sign detections are performed using a sliding window detector with a fixed square size of 1m x 1m, with overlapping grids shifted in 0.25 m increments in all directions. Points from 30 consecutive frames are accumualated for each classification, to obtain a fuller representation of each object being classified. After the signs are classified, a non-maximal suppression algorithm is run to cluster the sign predictions, using an alternative to mean shift [16] (see Figure 8). Finally, a weighted voting method is used to combine classification scores across time frames to produce a single classification score per location.

We then attempt to determine whether a given sign is a stop sign in a direction-invariant manner. To do this, we accumulate points and project them onto a RANSAC plane. We use Haar-type filters with a sliding window to determine the differential along the edges of the target sign. Because the absolute size of the object is known, scaling is not necessary.

Currently we detect signs at 89% precision, which significantly reduces the amount of manual effort required to annotate a map. In related ongoing work, we are exploring the algorithmic discovery of traffic lights, lane markers, crosswalks, and street signs so that the manual annotation of these features in drivable maps may eventually be replaced automated methods.

X. Conclusion

With the previously described realtime algorithms operating in concert, Junior has been able to drive autonomously for hundreds of miles in a variety of lighting, weather, and traffic conditions. Challenges including narrow roads, crosswalks, and intersections governed by traffic lights are now manageable. However, it remains necessary for a safety driver to be present at all times, and we are not yet able to drive for hours on end without occasionally switching to manual control due to unexpected events.

As an academic research lab, we have been focusing our efforts on scientifically interesting challenges with important practical implications. We consider tasks such as object detection and classification, precision localization and planning under uncertainty, and automatic calibration and environmental feature discovery, to be among the most algorithmically demanding topics that were not fully solved by any Urban Challenge entry or published work. Towards that end, in this paper we have presented several successful techniques that conquer these tasks.

Nevertheless, much work remains to be done before self-driving cars become a reality for commuters. Significant engineering effort, beyond that appropriate for a research lab, must go into a system to ensure maximal reliability and safety in all conditions. Sensors, of which several hundred thousand US dollars worth are used on our vehicle, are still prohibitively expensive for a consumer vehicle. Finally, the hardest perception and reasoning tasks still remain unsolved to date, as no autonomous vehicle has yet demonstrated an ability to understand and navigate construction zones, accident areas, and other unexpected scenarios at nearly the proficiency of a human driver.

References

[1] M. Montemerlo, J. Becker, S. Bhat, H. Dahlkamp, D. Dolgov, S. Ettinger, D. Haehnel, *et al.*, "Junior: The Stanford Entry in the Urban Challenge," *Journal of Field Robotics*, vol. 25(9), pp. 569–597, 2008.

[2] E. Dickmanns, "Vision for ground vehicles: history and prospects." *IJVAS*, vol. 1(1), 2002.

[3] J. Levinson and S. Thrun, "Unsupervised Calibration for Multi-beam Lasers," in *International Symposium on Experimental Robotics*, 2010.

[4] ——, "Robust Vehicle Localization in Urban Environments Using Probabilistic Maps," in *International Conference on Robotics and Automation*, 2010.

[5] J. Levinson, M. Montemerlo, and S. Thrun, "Map-Based Precision Vehicle Localization in Urban Environments," in *Robotics Science and Systems*, 2007.

[6] A. Teichman, J. Levinson, and S. Thrun, "Towards 3D Object Recognition via Classification of Arbitrary Object Tracks," in *International Conference on Robotics and Automation*, 2011.

[7] M. Werling, J. Ziegler, S. Kammel, and S. Thrun, "Optimal trajectory generation for dynamic street scenarios in a frenet frame," in *ICRA*, 2010, pp. 987–993.

[8] P. Martin, P. Rouchon, and J. Rudolph, "Invariant tracking," *ESAIM: Control, Optimisation and Calculus of Variations*, vol. 10, no. 1, pp. 1–13, 2004.

[9] J. Ziegler, M. Werling, and J. Schroder, "Navigating car-like robots in unstructured environments using an obstacle sensitive cost function," in *2008 IEEE Intelligent Vehicles Symposium*, 2008, pp. 787–791.

[10] C. Urmson, J. Anhalt, D. Bagnell, C. Baker, D. Ferguson, *et al.*, "Autonomous driving in urban environments: Boss and the urban challenge," *Journal of Field Robotics*, vol. 25, pp. 425–466, 2008.

[11] T. D. Gillespie, *Fundamentals of Vehicle Dynamics*. SAE Interational, 1992.

[12] J. C. Gerdes and E. J. Rosseter, "A unified approach to driver assistance systems based on artificial potential fields," in *Proceedings of the ASME International Mechanical Engineering Congress and Exposition*, 1999.

[13] B. D. O. Anderson and J. B. Moore, *Optimal Control: Linear Quadratic Methods*. Prentice-Hall, 1989.

[14] J. Levinson, J. Askeland, J. Dolson, and S. Thrun, "Traffic Light Localization and State Detection," in *International Conference on Robotics and Automation*, 2011.

[15] N. Dalal and B. Triggs, "Histograms of oriented gradients for human detection," in *Computer Vision and Pattern Recognition, 2005. CVPR 2005. IEEE Computer Society Conference on*, vol. 1, 2005, pp. 886 –893 vol. 1.

[16] D. Comaniciu and P. Meer, "Mean shift: a robust approach toward feature space analysis," *Pattern Analysis and Machine Intelligence, IEEE Transactions on*, vol. 24, no. 5, pp. 603 –619, May 2002.